Available online at www.sciencedirect.com
SCIENCE DIRECT®
International Journal of Heat and Fluid Flow 26 (2005) 459–473
International Journal of HEAT AND FLUID FLOW
www.elsevier.com/locate/ijhff

Three-dimensional numerical study of heat transfer characteristics of plain plate fin-and-tube heat exchangers from view point of field synergy principle

Y.L. He, W.Q. Tao *, F.Q. Song, W. Zhang

State Key Laboratory of Multiphase Flow in Power Engineering, School of Energy & Power Engineering, Xi'an Jiaotong University, Xi'an, Shaanxi 710049, China

Received 5 June 2003; accepted 26 November 2004
Available online 2 March 2005

Abstract

In this paper, 3-D numerical simulations were performed for laminar heat transfer and fluid flow characteristics of plate fin-and-tube heat exchanger. The effects of five factors were examined: *Re* number, fin pitch, tube row number, spanwise and longitudinal tube pitch. The Reynolds number based on the tube diameter varied from 288 to 5000, the non-dimensional fin pitch based on the tube diameter varied from 0.04 to 0.5, the tube row number from 1 to 4, the spanwise tube pitch S_1/d varies from 1.2 to 3, and the longitudinal tube pitch S_2/d from 1.0 to 2.4. The numerical results were analyzed from the view point of field synergy principle, which says that the reduction of the intersection angle between velocity and fluid temperature gradient is the basic mechanism to enhance convective heat transfer. It is found that the effects of the five parameters on the heat transfer performance of the finned tube banks can be well described by the field synergy principle, i.e., the enhancement or deterioration of the convective heat transfer across the finned tube banks is inherently related to the variation of the intersection angle between the velocity and the fluid temperature gradient. It is also recommended that to further enhance the convective heat transfer, the enhancement techniques, such as slotting the fin, should be adopted mainly in the rear part of the fin where the synergy between local velocity and temperature gradient become worse.

Keywords: Plate fin-and-tube surface; Field synergy principle; Numerical simulation

1. Introduction

Plate fin-and-tube heat exchangers are employed in a wide variety of engineering applications, for instance, in air conditioning units, process gas heater and coolers, compressor intercoolers, etc. There have been a number of studies on the pressure drop and heat transfer characteristics of the finned tube heat transfer surfaces. For the purpose of the present study, only the very recent numerical work is briefly reviewed here. Jang et al. (1996) performed 3-D computations for laminar flow and heat transfer of plate fin-and-tube heat exchangers of both staggered and in-line configurations. It was found that the average Nusselt number is decreased as the number of tube row is increased from 1 to 6. However, when the row number is greater than 4, the effect of the row number on the averaged Nusselt number becomes very weak. In order to take advantages of less computational memory of two-dimensional numerical computations and make uses of them for actual finned tube heat exchangers, Xi et al. conducted a comparative study for two-row finned surface to clarify the differences in numerical results between 2-D and 3-D

* Corresponding author.
E-mail address: wqtao@mail.xjtu.edu.cn (W.Q. Tao).

0142-727X/$ - see front matter © 2005 Elsevier Inc. All rights reserved.
doi:10.1016/j.ijheatfluidflow.2004.11.003

computations (Xi et al., 1997). They found that the value of heat transfer coefficient from 2-D model is larger than that of a 3-D finned tube model, but the variation of the heat transfer performance with the fin length of 2-D simulation shows a qualitative agreement with that of the 3-D case. Therefore they suggested that it would be possible to use the 2-D model for qualitative predictions of flow and heat transfer performance of the 3-D finned tube heat exchangers. Tsai and Sheu Tony (1998) made 3-D numerical studies for two-row staggered finned tube exchanger. The major purpose of their study was emphasized on the flow structure. Their study showed that the topological theory is a useful tool for exploring the details of the flow structure. Mendez et al. (2000) examined the influence of fin spacing on the heat transfer coefficients of the tube side of a single-row finned tube heat exchanger through flow visualization and numerical computation. The variation trend of the flow pattern with the non-dimensional fin spacing is revealed. With the increase of this parameter, the flow pattern varies from Hele–Shaw to horseshoe vortex followed by the formation of a separated region behind the tube. These studies have provided us with very useful information about the flow and heat transfer characteristics of finned tube heat transfer surfaces.

This paper revisits the problem from very different point of view. Most of the existing numerical studies were performed with emphasis placed on the parametric study. The parameters examined includes the fin pitch, the tube row number, the Reynolds number, and the spanwise and longitudinal tube pitches. By varying one of these parameters while keeping the others the same, the heat transfer rate of the finned tubes varies, either increases or decreases. In all the previous studies, these results were just described, or with some explanations from convective heat transfer and/or fluid flow considerations. Here a question may be put forward: what is the common essence responsible for the enhancement or deterioration of the convective heat transfer when these parameters are varying? Within the authors' knowledge this problem has not been addressed yet in the existing literatures related to the finned tube heat transfer.

In 1998, Guo and co-workers (Guo et al., 1998; Wang et al., 1998) proposed a novel concept about the enhancement of convective heat transfer. They worked with the energy governing equation of the parabolic flow and showed that the reduction of the intersection angle between the velocity and temperature gradient can effectively enhance the heat transfer. Later, Tao et al. (2002a,b) demonstrated that this idea is also valid for elliptic flow if the fluid Prandtl number is not too small. This concept is now called as field synergy principle, since the word "synergy" means cooperative action of two forces or the like (Guralnik, 1979). An extension of the field synergy principle to more general transport phenomena was made by He (2002) and He et al. (2004), and a comprehensive review on the recent development of the study on the field synergy principle was conducted by Tao and He (2002) and He and Tao (2002).

This paper examines the effects of five parameters on the heat transfer of finned tube bank from the point view of field synergy principle. Numerical simulation for plain plate fin-and-tube heat transfer surface is conducted and the volume average intersection angle between the velocity and temperature gradient within the computational domain is determined. Then the heat transfer variation trend with the parameter studied is compared with the variation trend of the average intersection angle with the same parameter to see if the two trends are consistent with the new concept. It turns out to be that it is the case.

In the following, the concept of the field synergy principle for the elliptic flow is first briefly reviewed for readers' convenience, followed by a brief description of the physical and numerical models and the numerical methods adopted. Then the details of the computational results are provided, emphasizing the comparison between the numerical results with the concept of the field synergy principle. Discussion is also made on the usefulness of the field synergy principle in design of enhanced heat transfer surface. Finally some conclusions are drawn.

2. Brief introduction to the field synergy principle

For an arbitrary computational domain within which an elliptic flow exists (Fig. 1), the energy governing equation can be written as:

$$\rho c_p\left(u\frac{\partial T}{\partial x}+v\frac{\partial T}{\partial y}+w\frac{\partial T}{\partial z}\right)=\lambda\left(\frac{\partial^2 T}{\partial x^2}+\frac{\partial^2 T}{\partial y^2}+\frac{\partial^2 T}{\partial z^2}\right) \quad (1)$$

Here the flow is assumed to be in a steady state and the fluid is of constant properties. In Fig. 1 only a cross-section of the 3-D domain is presented. For the simplicity of presentation while not losing the generality, the dimension normal to the cross-section may be assumed to be unity. The convective term can be re-written in

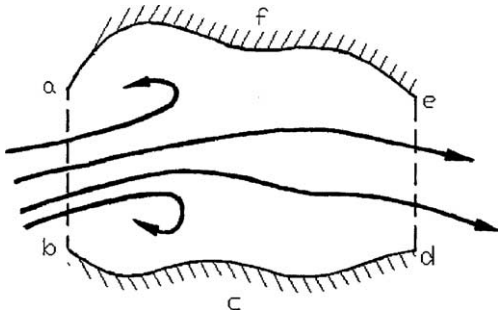

Fig. 1. An arbitrary computational domain for elliptic flow.

the form of inner product of the velocity vector and the temperature gradient, then we have

$$\rho c_p(\vec{U}\cdot \mathrm{grad}T) = \lambda\nabla^2 T \tag{2}$$

Integrating Eq. (2) over the computational domain shown in Fig. 1 and incorporating the Gauss law of reduction of integral dimensionality for the diffusion term, we have

$$\int_\Omega \rho c_p(\vec{U}\cdot \mathrm{grad}T)\,\mathrm{d}A - \int_{ab}\lambda\vec{n}\cdot\nabla T\,\mathrm{d}s - \int_{de}\lambda\vec{n}\cdot\nabla T\,\mathrm{d}s = \int_{bcd}\lambda\vec{n}\cdot\nabla T\,\mathrm{d}s + \int_{efa}\lambda\vec{n}\cdot\nabla T\,\mathrm{d}s \tag{3}$$

where *ab*, *bcd*, *de* and *efa* are the boundaries of the computational domain, and $\vec{n}$ is the outward normal to the computation domain boundary. The two terms on the right side are the heat transfer rate along the solid wall between the fluid and solid, representing the convective heat transfer rate. The first term on the left hand is the energy transferred due to the motion of the fluid, while the second and third terms on the left hand side are the heat conduction in the fluids. For flow with Peclet number greater than 100, these terms can be totally neglected compared the first term (Kays and Crawford, 1980). Thus we have

$$\int_\Omega \rho c_p(\vec{U}\cdot \mathrm{grad}T)\,\mathrm{d}A = \int_{bcd}\lambda\vec{n}\cdot\nabla T\,\mathrm{d}s + \int_{efa}\lambda\vec{n}\cdot\nabla T\,\mathrm{d}s \tag{4}$$

The inner production $(\vec{U}\cdot \mathrm{grad}T) = |\vec{U}||\mathrm{grad}T|\cos\theta$, here θ is the local intersection angle between the local velocity vector and the temperature gradient. Hence, the value of the integration or the strength of the convection heat transfer depends not only on the velocity, the temperature gradient, but also on their intersection angle, i.e., the synergy between velocity and the temperature gradient. Obviously, when the velocity and the temperature gradient is in full synergy, i.e., they are in the same direction, then the increase in velocity is directly proportional to the increase in heat transfer rate, the most efficient situation one can get for convective heat transfer. In this sense, it is the non-zero—degree intersection angle of velocity and temperature gradient that deteriorate the convective heat transfer in some extent. Therefore it is quite clear that for a given flow rate and temperature difference between fluid and heat transfer surface, we should keep the synergy between velocity and temperature gradient as good as possible in order to enhance heat transfer.

Thus the major concept of the field synergy principle for the enhancement of convective heat transfer may be stated as follows: the better the synergy of velocity and temperature gradient, the higher the convective heat transfer rate under the same other conditions. The synergy of the two vector fields or the three scalar fields (the module of velocity, the module of temperature gradient and the cosine of their intersection angle) implies that (a) the intersection angle between the velocity and the temperature gradient should be as small as possible, i.e., the velocity and the temperature gradient should be as parallel as possible; (b) the local values of the three scalar fields should all be simultaneously large, i.e., larger values of $\cos\theta$ should correspond to larger values of the velocity and the temperature gradient. Better synergy among such three scalar fields will lead to a larger value of the Nusselt number.

According to this principle the essence of enhancing convective heat transfer is to reduce the intersection angle. In Tao et al. (2002b) it has been shown that the three existing methods for augmentation of convective heat transfer (reducing the thickness of thermal boundary layer, increasing the disturbance in fluid, and increasing the velocity gradient at the solid wall) can be unified by the field synergy principle. This means that the essence of all the enhancement techniques of the single phase heat transfer is to reduce the intersection angle between velocity and temperature gradient.

3. Physical model and mathematical formulation

The fluid is assumed to be incompressible with constant property and the flow is laminar and in steady-state. Since the major task of the present study is to examine the feasibility of the field synergy principle in the heat transfer process of flow across finned tube banks, rather than obtaining accurate heat transfer rate, further simplification is made for the fin. It is considered to be a plain plate of constant wall temperature. This implies that the fin efficiency is assumed to be equal to 1. This simplification can also be understood as the assumption of isothermal wall boundary condition.

In our numerical simulation, the Reynolds number varied from 288 to 5000. A question may be raised as whether the laminar and steady model works for such high Reynolds number. Our considerations are as follows. First, the experimental observations and data for the flow regime transition in such complicated cases are not so well-accumulated and definite, as the ones for the flow in a simple channel. If we regard the flow between two adjacent fin surfaces as a channel flow, the transition Reynolds number may take the value around 2300, with the double spacing between the two fin surfaces as the reference dimension for the Reynolds number (Incropera and DeWitt, 2002). It is to be noted that the tube diameter is usually 10 times of the fin spacing, thus the value of $Re_\delta = 2300$ (based on the fin spacing) corresponds to the value around 10 000 based on the tube diameter, Re_d. If we take the flow between two adjacent fin surfaces as the flow past a cylinder, then experimental data have shown that the turbulent flow occurs for $Re_d \geqslant 2\times 10^5$ (Incropera and DeWitt,

2002). Therefore from the above discussion, the value of flow transition Reynolds number for the cases studied is still a problem open to discussion; Second, from the engineering point of view, the most important information is the averaged friction factor and the Nusselt number. For example, for flow past a single cylinder, flow visualization has shown that when the Reynolds number beyond 100, unsteady wake occurs behind the cylinder (Bejan, 1993). However, this fact does not prevent the usage of the time averaged drag coefficient and Nusselt number in engineering calculation. Third, recently, Xue and Min performed a comparative study for flow in corrugated channels by using steady and transient models with the same conditions (Xue and Min, 2004). They found that when the flow reaches periodic unsteady regime, it is appropriate to use steady model to predict the averaged Nusselt number and friction factor, and use of unsteady model is unnecessary because the unsteady model yields nearly the same Nusselt number and friction factor as the steady model. Stimulated by their results, the present authors also conducted a comparison between steady and unsteady models for $Re = 5000$ by adopting the commercial software FLUENT 6.0, and it is found that the difference in the averaged Nusselt number between these two models is only about 0.35%. Finally, many numerical studies in the existing literature adopted the steady and laminar models for plate fin-and-tube heat transfer surfaces when $Re_d > 1000$, and reasonably good results are obtained. To name a few, the following are some examples. Jang and Yang (1998) conducted numerical studies on plain plate fin-and-tube surfaces with elliptic and round tubes, by using laminar and steady model. In their simulation the maximum frontal velocity is about 7.0 m/s, which corresponds a maximum $Re_d = 1.0 \times 10^4$. For louvered fin coils, there have been some numerical studies including Ei-Hawat et al. (2001), Liu et al. (2001), which used laminar steady numerical model. In Ei-Hawat et al. (2001) the maximum Reynolds number based on the tube diameter is around 2900, in Liu et al. (2001) the upper limit of Re_d is about 1800. For wavy fin configuration, Min and Webb (2001), Comini and Groce (2001) adopt laminar steady model, and the values of Re_d were both larger than 1000. To further enhance our consideration for the steady model computation, the present authors also performed the comparison between steady and unsteady computation for the case of Reynolds number = 5000 by using the self-developed code. The results will be presented in the section of computational results and discussion.

The schematic diagram of a plain plate fin-and-tube heat exchanger is shown in Fig. 2a. Fig. 2b gives a top view of the two-row heat exchanger. As the total fin construction has the symmetry characters in the y-direction, a calculation element was defined as the shadowed part of the figure. Fig. 3 presents the four configurations of

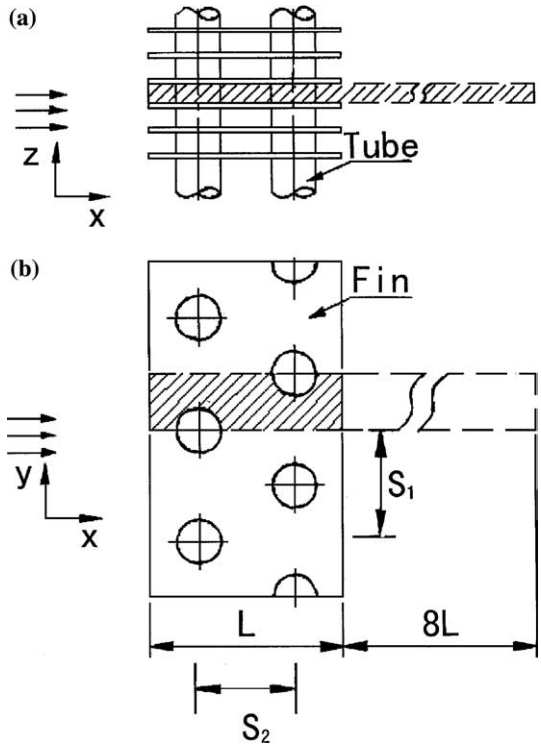

Fig. 2. Schematic of plate fin-and-tube heat exchanger.

finned tube banks studied. The grid systems for the four configurations are shown in Fig. 4. The actual computation domain was 9 times of the original heat transfer zone such that at the outer flow boundary no flow re-circulation exists and the local one-way method can be used for the numerical treatment of the outer flow boundary condition (Patanker, 1980; Tao, 2001). In the figure the downstream part of the computational domain is not fully presented in order to save the space. As can be observed there, at the rear extended part a much coarser grid was adopted to save the computing resource. In general the abrupt grid width change in the computing region should be avoided. A test of the effect of grid width variation from the last grid in fin area to that in the flow region situated after the fin area was then conducted at $Re = 1000$. It is found that the Nusselt number obtained from the grid system with gradual variation in the after fin region is 20.5, which is about 1.4% less than the results from the abrupt change system as shown in Fig. 4. The comparison study shows that the abrupt grid width change in the present simulation can be accepted, which saves computational time appreciably. The following fact may be used to account for such outcome: in the after fin region there is no heat transfer, and its existence is just for the adoption of the local one-way method to treat the outflow boundary condition. In addition, the effect of the pre-fin region is also conducted at the $Re = 1000$ for the two-row case. By adding a pre-fin region with a length of 2.3 times of the fin we obtained a value of the Nusselt number about 1.5%

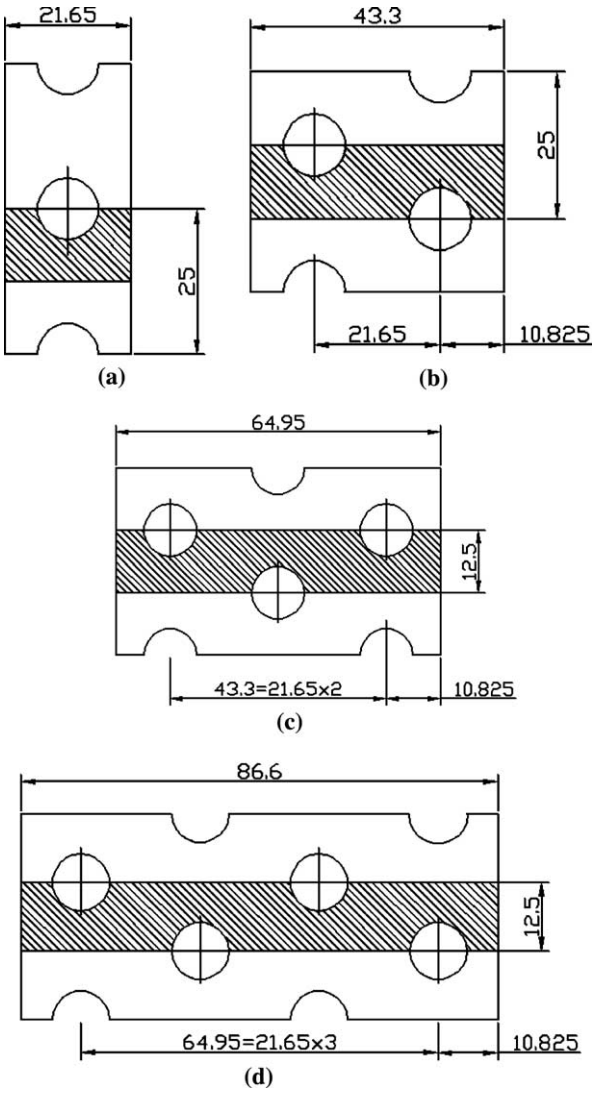

Fig. 3. Geometric parameters of the fin surfaces studied. Plain plate fin of single-tube row (a), two-tube rows (b), three-tube rows (c) and four-tube rows (d).

lower than that from the condition without the pre-fin region. Therefore, the pre-fin region effect may be neglected in the present study.

The governing equations for continuity, momentum and energy can be expressed as follows:

continuity equation:

$$\frac{\partial}{\partial x_i}(\rho u_i) = 0 \tag{5}$$

momentum equations:

$$\frac{\partial}{\partial x_i}(\rho u_i u_k) = \frac{\partial}{\partial x_i}\left(\mu \frac{\partial u_k}{\partial x_i}\right) - \frac{\partial p}{\partial x_k} \tag{6}$$

energy equation:

$$\frac{\partial}{\partial x_i}(\rho u_i T) = \frac{\partial}{\partial x_i}\left(\Gamma \frac{\partial T}{\partial x_i}\right) \tag{7}$$

where $\Gamma = \lambda/c_p$.

The velocity and temperature boundary conditions are as follows (Fig. 2).

Velocity:

Inlet boundary $u = C$, $v = w = 0$;	outlet boundary local one-way method;
Upper side and lower side	on the fin surface $u = v = w = 0$; in the rest part $\partial u/\partial z = \partial v/\partial z = \partial w/\partial z = 0$;
Left side and right side	on the tube surface $u = v = w = 0$; $v = 0$, $\partial u/\partial y = 0$, $\partial w/\partial y = 0$.
The four extended surfaces are all treated as symmetric.	

Temperature:

Inlet boundary $T = C$;	outlet boundary local one-way method;
Upper side and lower side	on the fin surface $T = T_w$; In the rest part $\partial T/\partial z = 0$;
Left side and right side	on the tube wall $T = T_w$; in the rest part $\partial T/\partial y = 0$;
The four surfaces of the extended region are all treated as symmetric.	

The local one-way method is a simple technique to treat the outflow boundary condition: set a zero value for the influence coefficient in the discretized equation for the control volume adjacent to the boundary. The only condition to adopt this technique is that there is no re-circulation at the outlet boundary. For details, Patanker (1980) and Tao (2001) may be consulted. Computations are conducted for four configurations of tube row numbers, with the number of tube row varying from 1 to 4 (Fig. 3). The body-fitted coordinate system is used to generate curvilinear coordinate systems by numerically solving the Poisson equation with proper control of the grid densities. The grid numbers are $62(x) \times 10(y) \times 10(z)$, $76 \times 12 \times 10$, $142 \times 20 \times 10$, $158 \times 22 \times 10$, respectively for the four cases as shown in Fig. 3. The generated grid system is shown in Fig. 4. The grid independence test has been made, and the numerical results obtained can be almost regarded as grid-independent as far as the average Nusselt number is concerned. Taken the two-row case as an example, six grid systems were tested. They are $30 \times 8 \times 10$, $45 \times 12 \times 10$, $60 \times 12 \times 10$, $76 \times 12 \times 10$,$90 \times 12 \times 10$, $105 \times 15 \times 10$. The average Nusselt number of the fourth grid system differs from that of the sixth by less than 0.5%, hence computation was based on this grid system. The effects of the variation of grid numbers in y, z directions are specially made with the finest grids of $32(y) \times 22(z)$. It is found that compared to the grid of

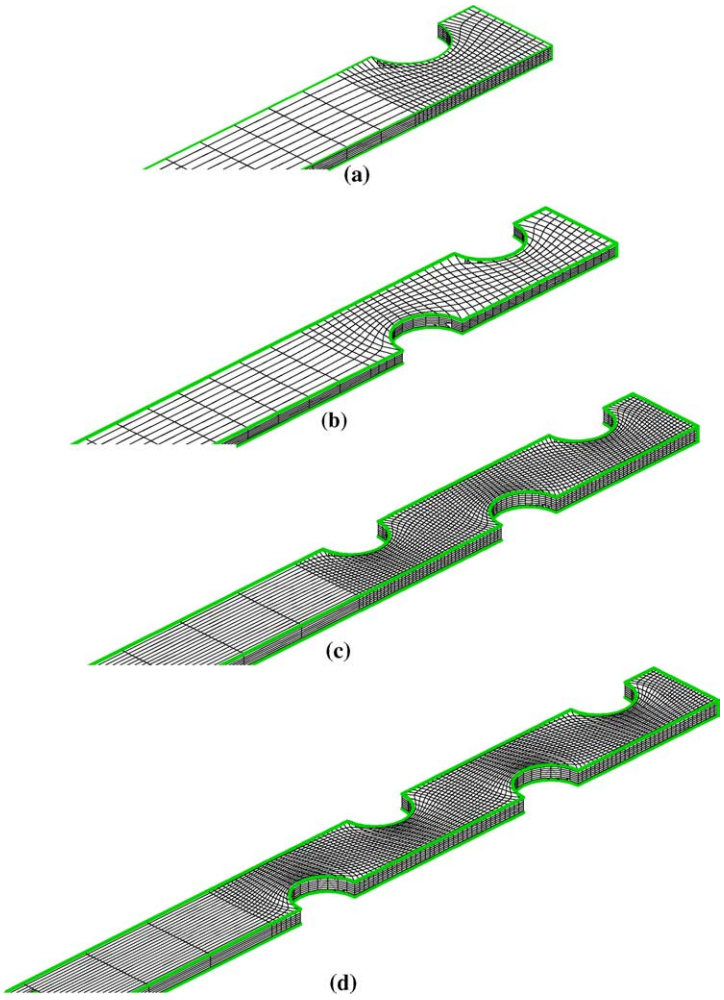

Fig. 4. Grid systems: (a) single-tube row, (b) two-tube row, (c) three-tube row and (d) four-tube row.

12×10, the maximum deviation in the Nusselt number is about 4% and the computational time is increased at least by an order of magnitude. Since the major aim of the present study is to conceptually examine the feasibility of the field synergy principle, rather than to get exact solution of the problem, the 12×10 grids in y and z direction is used.

The governing equations are discretized by the finite volume method, and the power-law scheme is used to discretize the convection–diffusion terms. The coupling of pressure and velocity is implemented by SIMPLER algorithm (Patanker, 1980; Tao, 2001).

4. Computational results and discussion

In the following the results of examining the effect of the Reynolds number, the fin pitch, the tube row number, and the spanwise and longitudinal tube pitch will be presented in order. For each examination, only one parameter varies and all the other conditions remain the same, except for the examination of the spanwise tube pitch, which will be specifically addressed later. The definitions of Re, average Nusselt number and friction factor are as follows.

$$Nu = \frac{h_m d}{\lambda}, \quad Re = \frac{u_{max} d}{v}, \quad f = \frac{\Delta p}{(1/2)\rho u_{max}^2 (L/d)} \tag{8}$$

where u_{max} is the fluid velocity at the minimum cross-section of the tube row, d is the outside diameter of the tube, L is the fin length along the flow direction, Δp is the total pressure drop over the fin length, and h_m is the mean heat transfer coefficient of the plate fin-and-tube, determined by the log-mean temperature difference between the wall temperature and the fluid inlet/outlet temperatures.

For the presentation of numerical results in terms of the field synergy principle, the following quantity is introduced:

$$M = \sum |\vec{U}||\mathrm{grad}T|/N \tag{9}$$

where N is the number of control volume covering the fin region.

Obviously, the value of M corresponds to the full synergy case, where all the intersection angle between velocity and temperature gradient becomes zero and the production of velocity vector and temperature gradient is the largest. For simplicity it will be called module production.

The local intersection angle is determined by the following equation

$$\theta = \cos^{-1}\frac{u\frac{\partial T}{\partial x} + v\frac{\partial T}{\partial y} + w\frac{\partial T}{\partial z}}{|\vec{U}||\mathrm{grad}T|} \tag{10a}$$

And from the local intersection angle the average intersection angle of the computation domain of the fin area can be obtained using numerical integration,

$$\theta_{\mathrm{m}} = \frac{\sum \theta_{i,j,k}\,\mathrm{d}v_{i,j,k}}{\sum \mathrm{d}v_{i,j,k}}, \tag{10b}$$

where $\mathrm{d}v_{i,j,k}$ is the volume element of the control volume (i,j,k).

4.1. Re number effect

The computation is conducted for the two-row case with the fin pitch and the tube diameter being 2 mm and 10 mm, respectively. The Re number ranges from 500 to 5000, and the corresponding frontal air velocity ranges from 0.464 m/s to 4.64 m/s.

Fig. 5a and b shows the relations of $Nu \sim Re$ and $f \sim Re$. They show that the Nu number increases with the increase of the Re number, while f decreases with the increase of the Re number. Furthermore, the increasing trend of Nusselt number with Re decreases with the increase in Re. These are the expected results.

In Fig. 6a the variation of the average intersection angle between velocity and temperature gradient is presented, and Fig. 6b provides the relation of $M \sim Re$. Fig. 6b shows that the value of M is almost proportional to the Reynolds number, but Fig. 6a indicates that the average intersection angle increases with Re, implying the deterioration of the synergy between velocity and temperature gradient. Thus it becomes clear that the decrease of the increasing trend of average Nu with Re with the increase of Reynolds number is resulted from the increase in the intersection angle between the velocity and the temperature gradient, i.e., the synergy between velocity and temperature gradient becomes worse and worse.

As a representation of the local distributions of the temperature, velocity and the intersection angle, their data are provided in Fig. 7 for the middle cross-section in the x–y plane between the upper and lower sides for Re = 1000. Since for the problem studied, the main flow

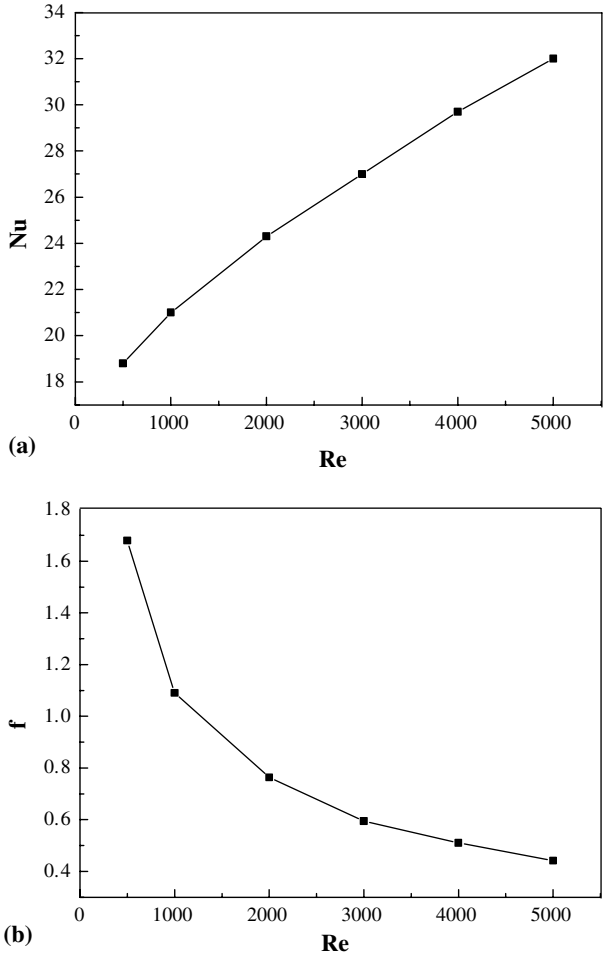

Fig. 5. Variation of Nu and f with Re.

is in the x-direction, and the component in the z-direction is of second order, our computational results show that the variation trend of the intersection angle in the x–y plane qualitatively agrees well with that of the 3-D intersection angle. For simplicity, we will adopt the numerical results in the middle plane as a representation in the following discussion. Fig. 7a shows that in the inlet part of the computational domain the isothermals of the temperature are almost perpendicular to the velocity vector, indicating a good synergy between the velocity and temperature gradient. The local intersection angle in this region is quite low, ranging from 2.1° to 18° except for the narrow region near the tube wall. While in the region behind the first tube, the isothermal becomes nearly parallel to the velocity vector, and the local intersection angle becomes much larger, ranging from 54° to 72°. Such predicted results provide us very useful information for the further improvement of the heat transfer performance of the plate fin-and-tube surface: if some enhancement technique, such as slotting the fin, is considered, then the slits should be first distributed in the region where the synergy is worse. For the case studied,

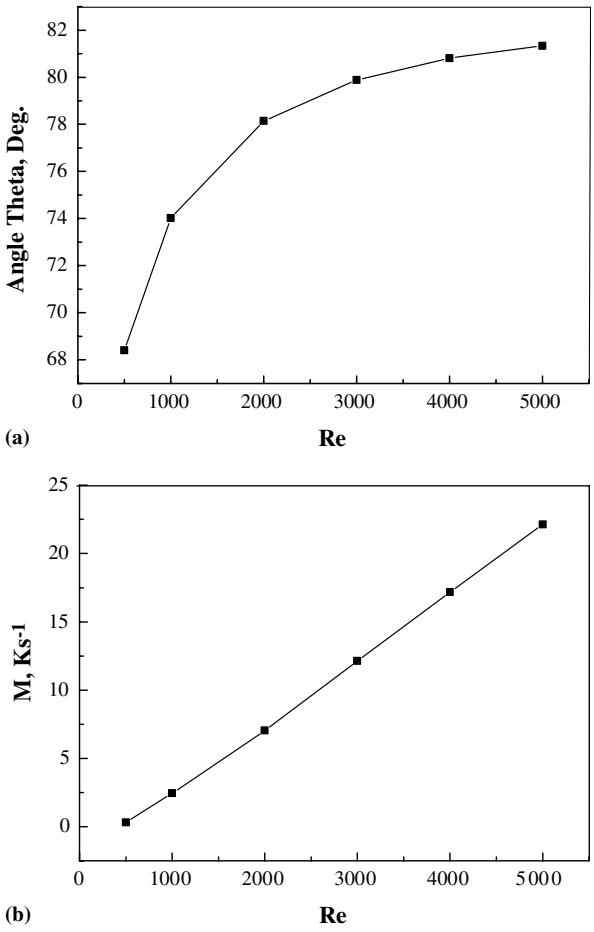

Fig. 6. The variation of intersection angle (a) and module production M (b) with Re.

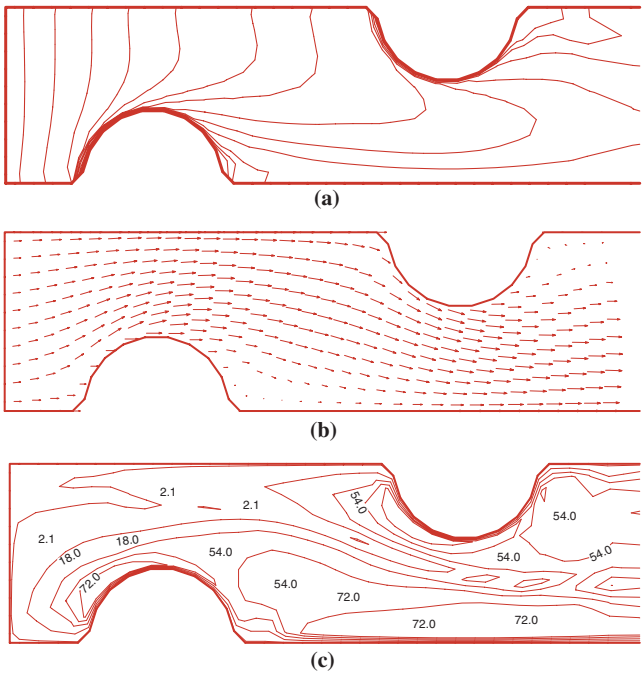

Fig. 7. Distributions of isothermal (a), velocity vector (b) and intersection angle (c) for $Re = 1000$.

they should be distributed behind the first tube, while in the inlet part of the fin no slits or less slits should be positioned, since the synergy of this region is good enough and no or less enhancement technique should be used in order to reduce the penalty in pressure drop. This finding can give an appropriate explanation for the experimental results provided in Kang and Kim (1999). Kang and Kim (1999) conducted experiments for revealing the effects of location of slits in the fin on the heat transfer performance of slotted plate fin-and-tube heat transfer surfaces. For a two-tube-row plate fin surface, they located the slots in two different places with other conditions all the same: one in the frontal part of the fin surface (i.e., upstream part), the other on the rear part of the fin surface (i.e., downstream part). Their experimental results show that the heat transfer performance of the slotted fin surface with slots located in the rear part is better than that in the frontal part. They did not provide the reasons. From the results of the present study, this is because in the downstream part the synergy between velocity and temperature is worse, therefore the enhancement technique can play a more significant role. Further researches in this regard conducted in the authors' group revealed that we may adopt this finding to design more efficient enhanced heat transfer surfaces (Cheng et al., 2004).

Fig. 8a–c gives the three fields for $Re = 5000$. The same discussion can be made as for the $Re = 1000$. Compared to Fig. 7, where $Re = 1000$, the zone in which the two fields are in worse synergy becomes larger, and so is the average intersection angle. Generally speaking, when the Re number changes from 1000 to 5000, the heat transfer rate is increased mainly due to the increase of the velocity that leads to almost a linear increase of the product of the modules of the velocity and the temperature gradient. On the other hand, with the increase in the Reynolds number the extent of Nu number increase with the increased Re number is decreased due to the deteriorated synergy between the velocity and the temperature gradient. It is interesting to note that the upper and lower boundary of the computational domain are symmetric lines for the temperature and velocity. The intersection angles of isothermals with these two boundaries presented in Fig. 8a are almost right angle, implying this symmetric character. In the figure some intersection angles deviate from right angle a bit, this is mainly because of some numerical imperfection, for example, the grid resolution near the boundary is not fine enough. In Fig. 8b, all the velocity vectors along the upper and lower boundaries are all parallel to the boundaries, indicating a nearly zero value of the velocity component normal to the boundaries, a basic feature of the velocity filed near a symmetric line.

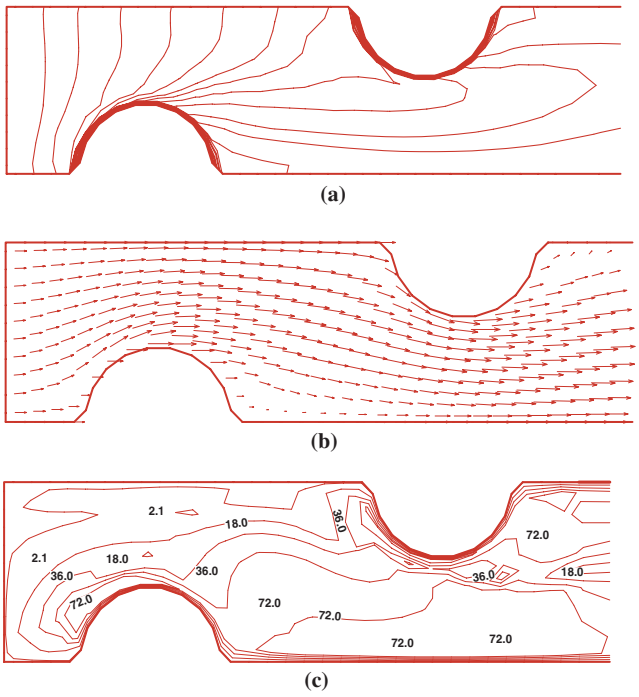

Fig. 8. Distributions of isothermal (a), velocity vector (b) and intersection angle (c) for $Re = 5000$.

Now the comparison study of steady model and unsteady model is presented. The computational conditions are as follows: the approaching velocity = 4.64 m/s, the inlet air temperature = 30 °C, tube row number = 2, the fin pitch = 2.2 mm, tube diameter = 10 mm. The fin thickness = 0.2 mm, $S_1/d = 2.5$, $S_2/d = 2.165$. For the unsteady computation, the initial temperature of the entire flow field was taken as 30 °C, and the initial flow velocity was zero. Although a fully implicit scheme was used for the unsteady computation, the time step was taken 1 s, a rather small time step in order to catch any possible oscillation during the time marching procedure. The grid system used was $136 \times 107 \times 24$. Because the unsteady computation is very time consuming, a newly proposed very efficient algorithm for dealing with the linkage between velocity and pressure, CLEAR, was adopted (Tao et al., 2004). The final results are quite encouraging. The unsteady computational results gradually approach the corresponding steady state computational results. The final results are compared in Table 1. From this comparison, we can be sure that the steady model adopted in this study is acceptable and reliable.

4.2. Fin pitch effect

For examining the fin pitch effect, the two-tube-row configuration is adopted. The fin pitch varies from 0.4 mm to 5 mm. The inlet flow velocity is taken as 2 m/s, and the rest parameters remain the same.

Table 1
Comparison study for two-row case with $Re = 5000$

Cases	Heat transfer coefficient (W/m^2 K)	Nusselt number	Domain averaged intersection angle (deg)
Steady	84.95	31.85	86.61
Unsteady	83.66	31.37	87.17
Relative difference (%)	1.54	1.54	0.64

Fig. 9a shows the relation of fin pitch and the Nu number. It can be seen that the Nu number reaches the maximum at the fin pitch of 0.6 mm. Departure from this value, either increase or decrease in fin pitch, leads to the decrease in the average Nusselt number. When the fin pitch is greater than 2.5 mm, the fin pitch has less effect on the average Nusselt number. In Fig. 9b the effect of fin pitch on the friction factor is presented, where a monotonic variation can be observed and an asymptotic pattern of $f \sim Re$ appears with the increase in fin pitch.

The field synergy presentations are provided in Fig. 10. It can be concluded from Fig. 10a that the average intersection angle is the minimum when the fin pitch is equal to 0.6 mm. A departure of fin pitch from this value leads to the increase in the angle. This implies that at the fin pitch of 0.6 mm we have the best synergy between the velocity and the temperature gradient for the case studied. This result agrees well with the field synergy principle. The variation of the product of the modules of the velocity and temperature gradient with the fin pitch is shown in Fig. 10b. It can be observed that with the increase in fin pitch the value of M first increases very fast, then the variation speed gradually slows down and finally almost keeps constant after the fin pitch reaches 3 mm. These variation patterns of $\theta_m \sim s$ and $M \sim s$ are very consistent with the variation of $Nu \sim s$ shown in Fig. 9a. The specific value of the optimum fin pitch revealed by this computation may not be applicable for a practical design since some assumptions are made, however, the qualitative result is of great importance to the design of fin configuration. Our results show that from the heat transfer rate between two adjacent fin surfaces the optimum fin pitch is the one where the synergy between the velocity and the temperature gradient is the best for the case studied. It may be noted that the existence of the optimum fin pitch is physically reasonable, however, the variation of curves in Figs. 9a and Fig. 10a seems a bit abrupt. The present authors have repeated the computations and the same results were obtained. One possible reason is the isothermal assumption of the fin surface. In practical situation the fin surface temperature distribution also depends on the flow velocity. The variation of the fin pitch affects the flow field and hence the fin surface

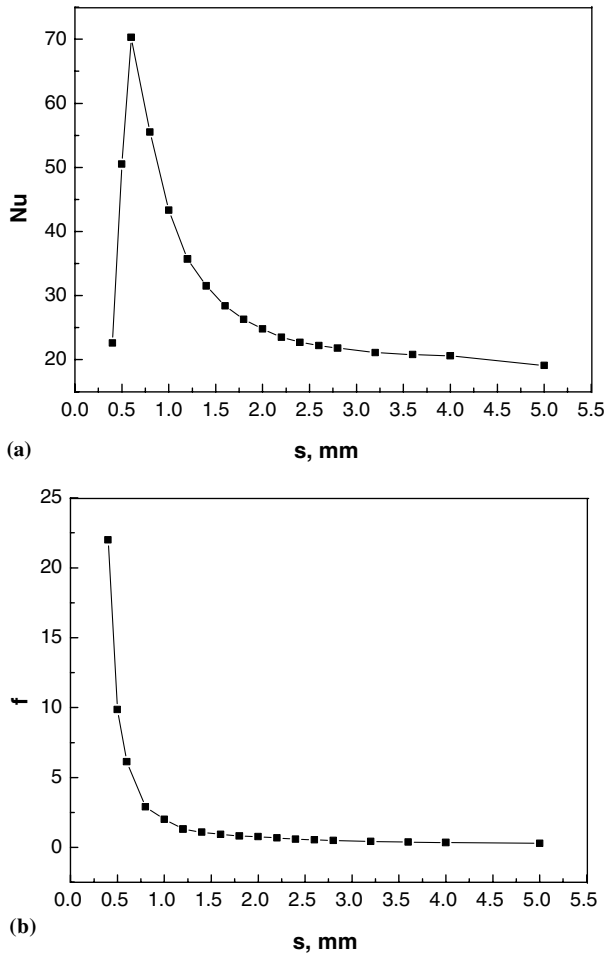

Fig. 9. Variation of average *Nu* and *f* with fin pitch.

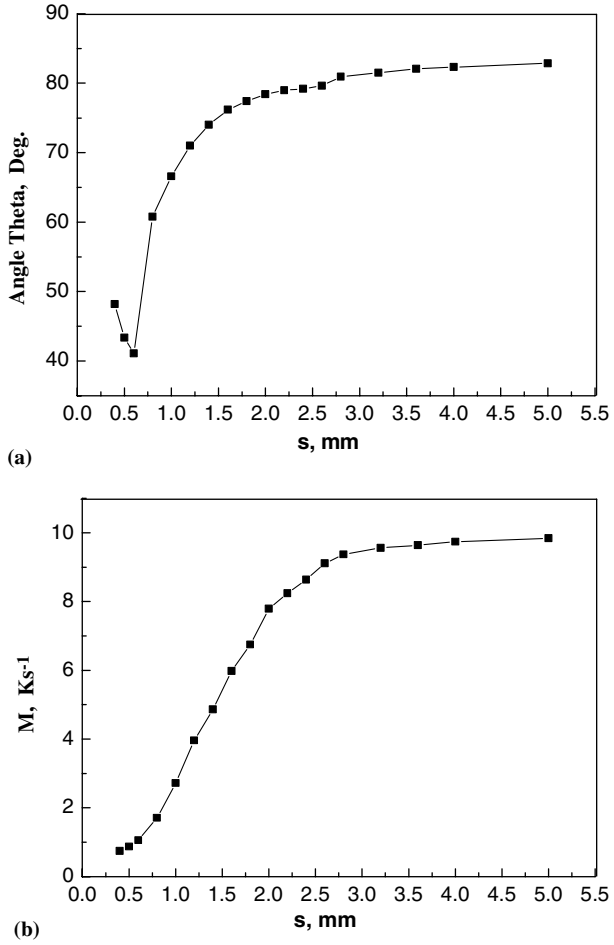

Fig. 10. Variation of average intersection angle and module production with fin pitch.

temperature distribution, which in turn affects the fluid temperature distribution. Such mutual influences may lead to a more mild variation of the heat transfer coefficient vs. fin pitch.

The distribution of the velocity, the temperature and the intersection angle at the middle cross-section for fin pitch equals 0.6 mm and 2.6 mm are provided in Figs. 11 and 12, respectively. It can be clearly observed that the local intersection angles for the case of $s = 2.6$ mm are all greater than that of $s = 0.6$ mm.

In the above presentation all the numerical results are relevant to the fin surface. Since the total heat transfer of the fin-and-tube surface composed of the heat transferred from fin and that from the tube, it may be interesting to show how many percentage of heat is transferred via the tube surface between the adjacent two fin surfaces. For the computational unit it is obvious that the largest percentage of the heat transfer via tube surface corresponds to the largest fin pitch, which is 5 mm in our study. Numerical results show that at the largest fin pitch this part of heat transfer is only about 5% of the total heat transfer rate, showing the rationality of our analysis.

4.3. Tube row number effect

For examining the effect of the tube row number, the inlet velocity is taken as 2 m/s and the fin pitch is 2.0 mm. The tube row number varies from 1 to 4.

Fig. 13a shows the variation of the average *Nu* number with the tube row number *n*. According to the figure, the *Nu* number decreases with the increasing tube row number, but the decreasing tendency is weakened gradually. The difference of *Nu* number of three and four rows is very subtle. Thereby if the tube rows number exceeds 3, the variation of the average heat transfer and friction factor is very small. These results are in qualitative agreement with that of Jang et al. (1996). Since in our study an ideal fin is assumed, and the focus is to analyze the affecting factors from the view point of the field synergy principle, no tempt was made to compare our numerical results to any test data. However, some qualitative conclusions, as the effect of the tube row number, are fully consistent with available test results.

The intersection angle is provided in Fig. 14a. The angle increases with the increasing tube row number,

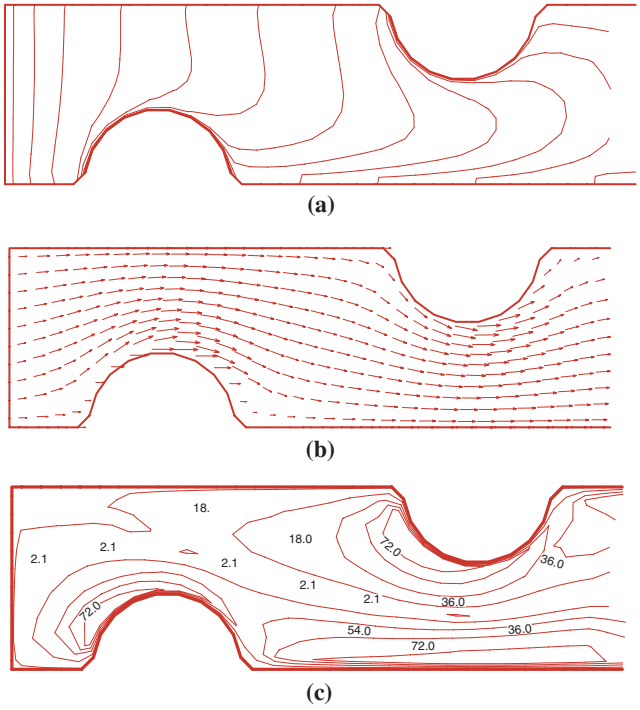

Fig. 11. Distributions of isothermals (a), velocity (b) and intersection angle (c) for $s = 0.6$ mm.

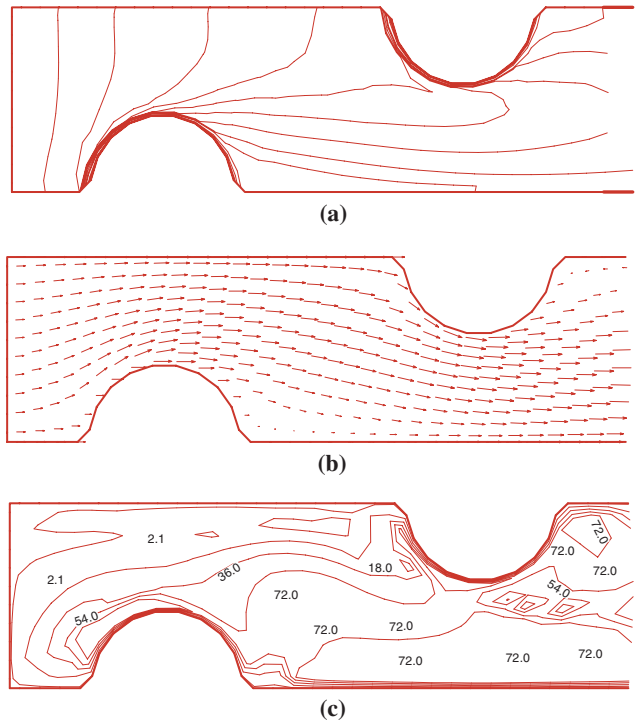

Fig. 12. Distributions of isothermals (a), velocity (b) and intersection angle (c) for $s = 2.6$ mm.

and after $n = 3$, the effect of n on θ_m is small. In Fig. 14b, it is shown that the product of modules of velocity and temperature gradient decreases with the tube row number. And after $n = 3$ the declining tendency is slowed down. These findings explain well why the average Nusselt number decreases with the tube row number and why the decrease tendency is slowed down after $n = 3$.

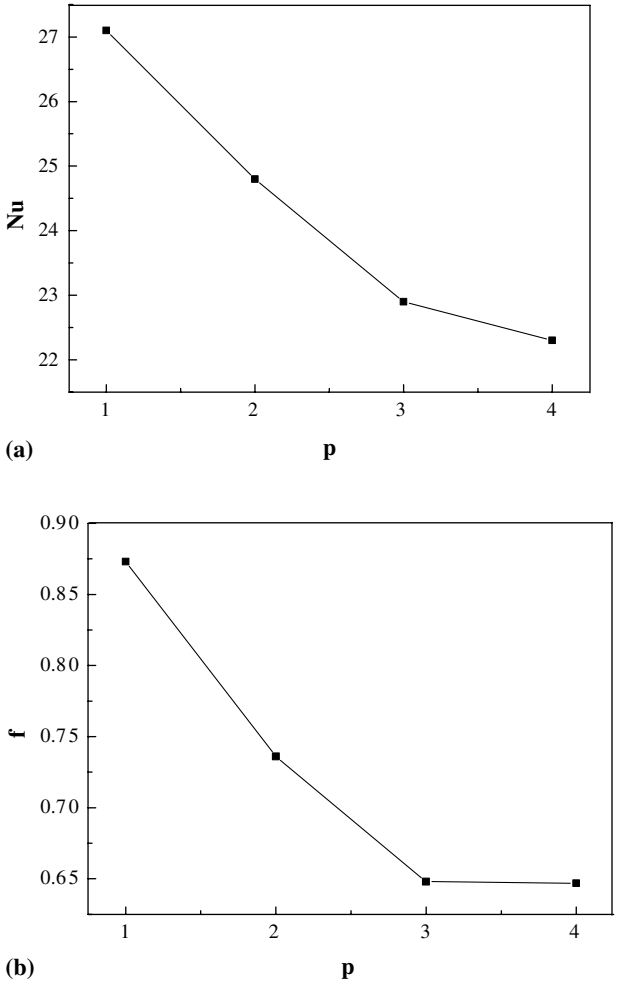

Fig. 13. Variation of *Nu* and *f* with tube row number.

The distributions of the temperature, velocity and intersection angle are presented in Figs. 15–18, respectively for one-row, two-row, three-row and four-row cases. By carefully inspecting the figures, it can be seen that the percentage of the region with larger intersection angle increases from one-row to four-row in order.

The above findings show that the smaller the tube row number the better the field synergy, hence, the better the heat transfer performance. Therefore, in practical applications, the tube row number less than 3 should be recommended.

4.4. Tube pitch effect

The effects of the spanwise tube pitch and the longitudinal tube pitch, S_1/d and S_2/d, on the average Nusselt number are presented in Fig. 19. For this study, computations were conducted for two-row tube bank under a

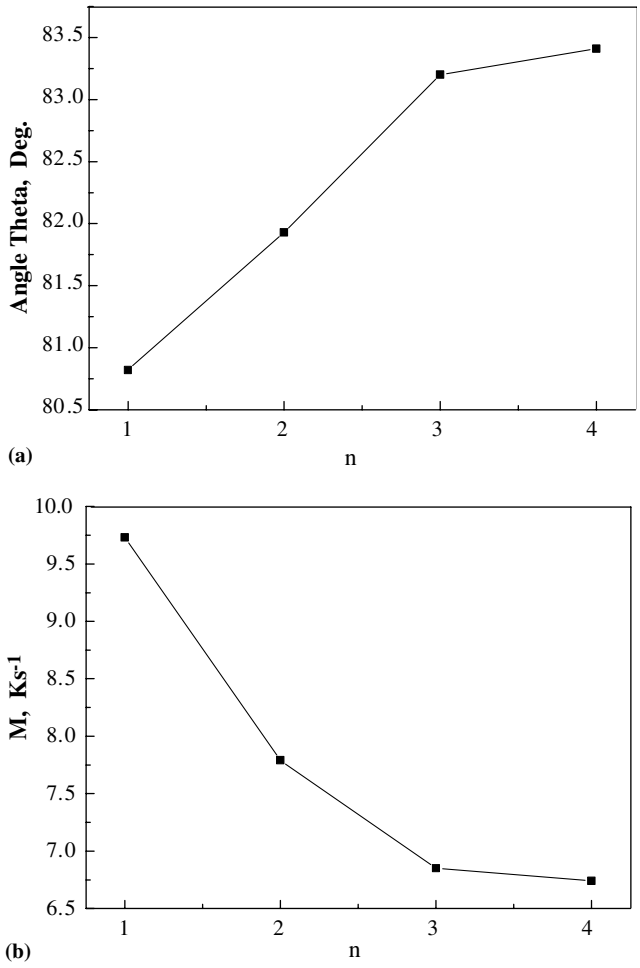

Fig. 14. Variation of average intersection angle and module production with tube row number.

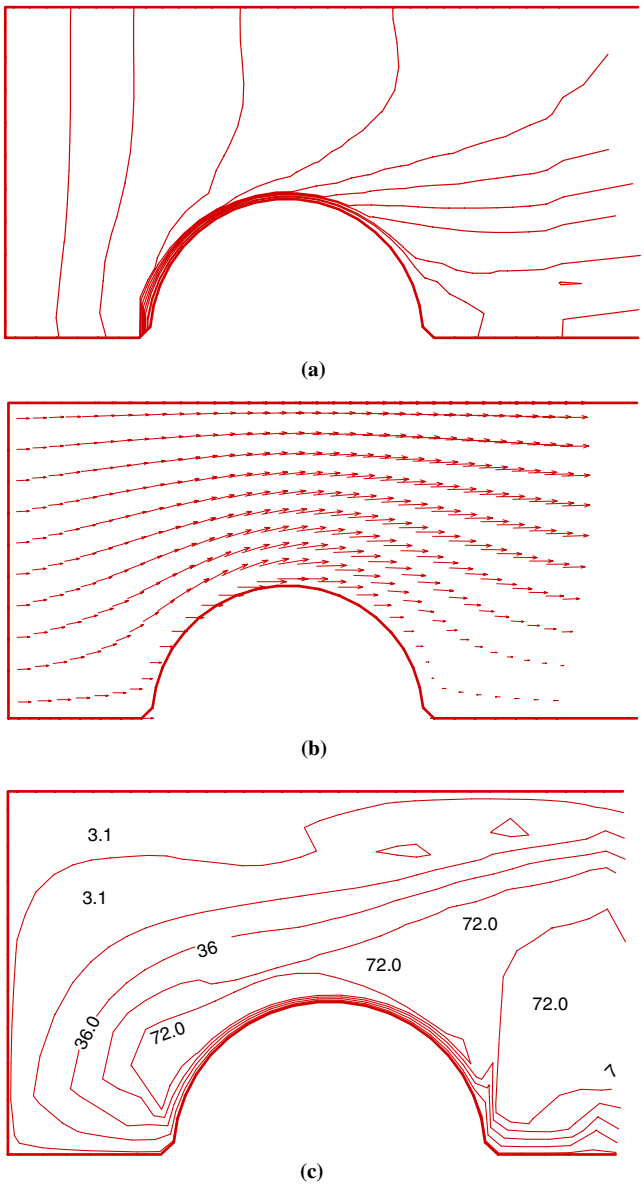

Fig. 15. Distributions of isothermals (a), velocity (b) and intersection angle (c) for single row.

fixed oncoming flow velocity, rather than a fixed Reynolds number since the value of u_{max} varies with the variation of S_1/d. The numerical data presented in Fig. 19 cover a Reynolds number from 288 to 1060. The following features may be noted. First, it can be clearly observed that with the increase in S_1/d or S_2/d, the average Nusselt number decreases; second, the effect of S_1/d on heat transfer is more appreciable than that of S_2/d. The corresponding variations of the intersection angle between the velocity and temperature gradient are presented in Fig. 20. It can be clearly observed that the variation trends of the intersection angle with S_1/d and S_2/d are fully consistent with that of the Nusselt number from the view point of the field synergy principle. Thus with a fixed oncoming flow velocity the increase in the tube pitches leads to worse synergy between velocity and temperature gradient.

Before concluding the presentation of our numerical results, some interesting points will be addressed. First, as can be seen above, the filed synergy principle is a fundamental concept to deepen our understanding of the convective heat transfer process. It differs from the concept of heat transfer coefficient in many ways. Here only one fact is cited to indicate the basic difference between them. As indicated above, Kang and Kim (1999) found that for the same number of slits, the fin with most slits in the downstream part has a higher heat transfer coefficient than that with most slits in the upstream part. With the concept of heat transfer coefficient, this is all what we can do for the test results. But from the field synergy principle, it is revealed that this basic difference comes from the different synergy between velocity and temperature gradient. And stimulated by this numerical finding, a new type of slotted fin surface was invented in Cheng et al. (2004). If we only have the concept of heat transfer coefficient, such invention would never be pos-

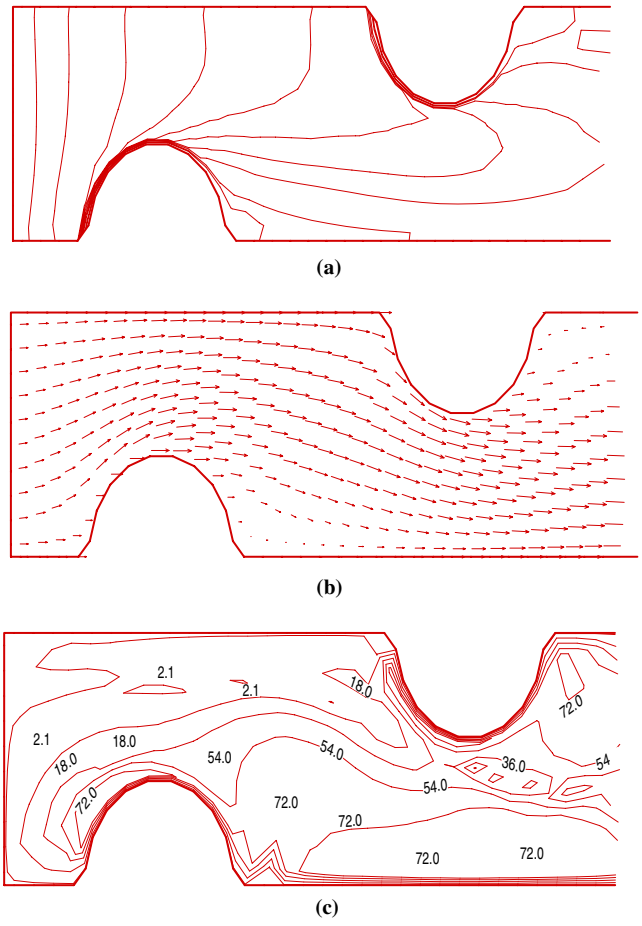

Fig. 16. Distributions of isothermals (a), velocity (b) and intersection angle (c) for two-row tube bank.

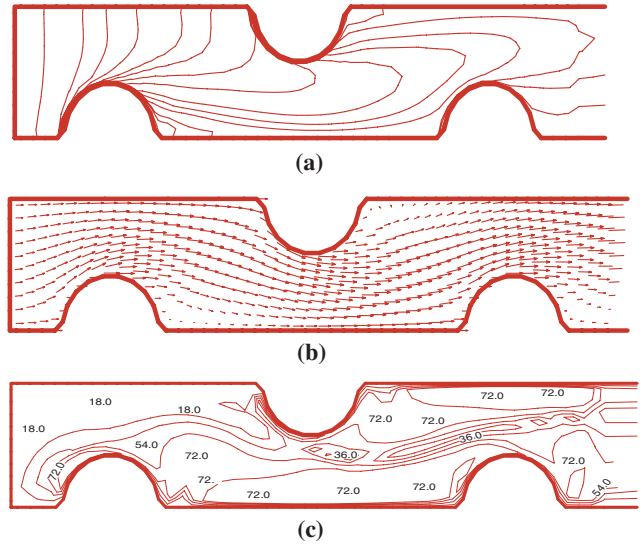

Fig. 17. Distributions of isothermals (a), velocity (b) and intersection angle (c) for three-row tube bank.

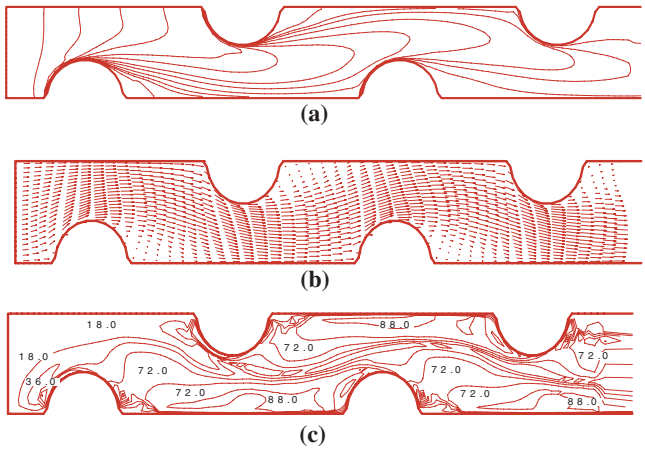

Fig. 18. Distributions of isothermals (a), velocity (b) and intersection angle (c) for four-row tube bank.

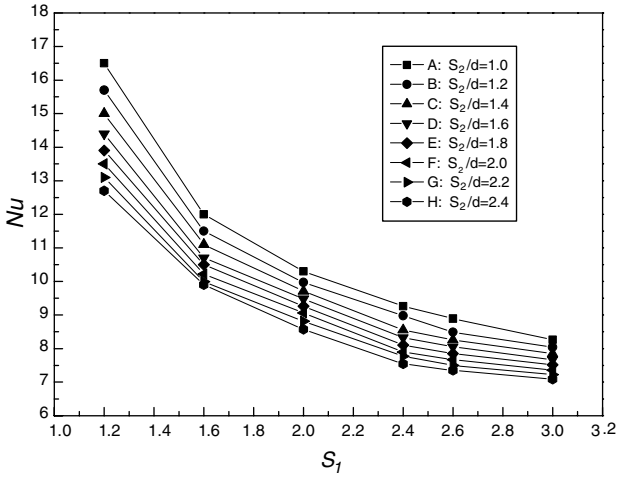

Fig. 19. Variations of Nu with S_1/d and S_2/d.

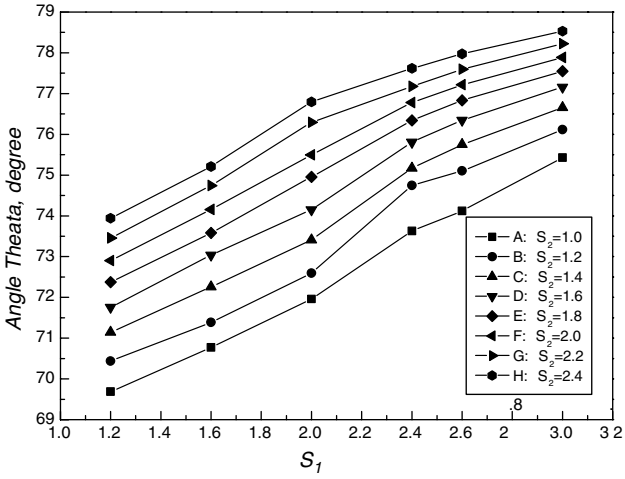

Fig. 20. Variation of intersection angle with S_1/d and S_2/d.

sible. Second, the concept of the field synergy principle is not only valid for laminar flow but also for turbulent flow. This has been demonstrated by numerical examples in Zeng and Tao (2004). Third, there are two full

synergy cases: $\cos\theta = 1$ ($\theta = 0°$) and $\cos\theta = -1$ ($\theta = 180°$). When $\cos\theta = 1$ ($\theta = 0°$) fluid is heated while $\cos\theta = -1$ ($\theta = 180°$) means cooling of the fluid. For these two cases the fluid flow is most efficient in that its flow direction is exactly the same direction along which the fluid is heated or cooled most efficiently. These are the two ideal situations, and in practice, the intersection angle varies from 0° to 180°. Thus for a specific situation, say, fluid is heated, the heat transfer surface should be designed in such a way that the local intersection angles are as small as possible. If the local intersection angle is less than 90°, the motion of fluid at the local region makes some positive contribution to the heating of the fluid (the local inner production is positive), while for the location where the local angle is larger than 90°, the local contribution is negative to the total heat transfer process. In this sense, the simple averaging method shown by Eq. (10b) works. Of course, some weighting factor may be adopted in the averaging process, and the present authors have made some preliminary investigations. It is found that the specific value of the averaged intersection angle differs from each other when different weighting factors are used for the same flow situation, however, the qualitative trends and conclusions are not affected. Even though further work is needed to find the most appropriate averaging method, in this paper for the simplicity of presentation the simple averaging method is used.

5. Conclusions

In this paper, 3-D numerical computations are conducted to reveal the effect of the Reynolds number, the fin pitch, the tube row number, the spanwise and longitudinal tube pitch on the average Nusselt number of finned tube banks. The numerical results are analyzed from the point view of the field synergy principle, seemingly first in the literature. The numerical results obtained in this study show that the heat transfer performance of the finned tubes can well be described by the field synergy principle, indicating once again the feasibility of the new concept. To be specific, the following conclusions can be made.

1. The increase of *Re* number leads to the increase of the *Nu* number. The enhancement of heat transfer is due to the increase of the module product of velocity and temperature gradient. However, the synergy between the velocity and the temperature gradient becomes worse and worse with the increase of the Reynolds number, leading to a less increasing tendency of *Nu* with *Re*.
2. There exists an optimum fin pitch at which the *Nu* number is the maximum. Both average intersection angle and the module product show an asymptotic tendency with the increase of fin pitch, leading to the insensitivity of the Nusselt number with the increase of fin pitch beyond a certain value of the fin pitch.
3. The average Nusselt number decreases with the increase of tube row number. The less the tube row number, the better the field synergy. For practical applications, a tube row number less than 3 is recommended from the field synergy principle.

Acknowledgments

The work is supported by the National Natural Science Foundation of China (No. 50425620, 50476046), a Foundation for the Author of National Excellent Doctorial Dissertation of PR China, and RFDP20030698015. The authors' thanks also go to Mr. Z.G. Qu and J.F. Zhang for their help in the computation of the unsteady case.

References

Bejan, A., 1993. Heat Transfer. John Wiley & Sons, New York, pp. 265–266.

Cheng, Y.P., Qu, Z.G., Tao, W.Q., He, Y.L., 2004. Numerical design of efficient slotted fin surface based on the field synergy principle. Numer. Heat Transfer Part B 45, 517–538.

Comini, G., Groce, G., 2001. Convective heat and mass transfer in tube-fin heat exchangers under dehumidifying conditions. Numer. Heat Transfer A 40, 5790–5799.

Ei-Hawat, S.M., Heikal, M.R., Sazhin, S.S., 2001. An improved three-dimensional numerical model of flow and heat transfer over louver fin arrays. Int. J. Heat Exchangers 11, 37–44.

Guo, Z.Y., Li, D.Y., Wang, B.X., 1998. A novel concept for convective heat transfer enhancement. Int. J. Heat Mass Transfer 41, 2221–2225.

Guralnik, D.B., editor-in-chief, 1979. WEBSTER'S New Word Dictionary of the American Language. 2nd college edition. William Collins Publishers, Inc., Cleveland, 1444.

He, Y.L., 2002. Theoretical and Experimental Investigations on the Performance Improvements of Split-Stirling Cryocooler and Pulse Tube Refrigerator. Ph.D. Thesis, Xi'an Jiaotong University.

He, Y.L., Tao, W.Q., 2002. Field synergy principle and its application in enhancing convective heat transfer and improving performance of pulse tube refrigerator, Part II. J. Xi'an Jiaotong Univ. 36, 1106–1110.

He, Y.L., Wu, M., Tao, W.Q., Chen, Z.Q., 2004. Improvement of the thermal performance of pulse tube refrigerator by using a general principle for enhancing energy transport and conversion processes. J. Appl. Therm. Energy 24, 79–93.

Incropera, F.P., DeWitt, D.P., 2002. Fundamentals of Heat and Mass Transfer, fifth ed. John Wiley & Sons, New York, pp. 408, 495.

Jang, Jiin-Yuh, Yang, Jyh-Yau, 1998. Experimental and 3-D numerical analysis of the thermal-hydraulic characteristics of elliptic finned-tubes heat exchangers. Heat Transfer Eng. 19 (4), 55–67.

Jang, J.Y., Wu, M.C., Chang, W.J., 1996. Numerical and experimental studies of three-dimensional plate-fin and tube heat exchanger. Int. J. Heat Mass Transfer 39, 3057–3066.

Kang, H.C., Kim, M.H., 1999. Effect of strip location on the air-side pressure drop and heat transfer in strip fin-and-tube heat exchanger. Int. J. Refrig. 22, 302–312.

Kays, W.M., Crawford, M.E., 1980. Convective Heat and Mass Transfer. McGraw-Hill Book Company, New York, pp. 107, 246.

Liu, J.S., Liu, M.S., Liaw, J.S., Wang, J.S., 2001. A numerical investigation study of louvered fin-and-tube heat exchangers having circular and oval tube configuration. Int. J. Heat Mass Transfer 44, 4235–4243.

Mendez, R.R., Sen, M., Yang, K.T., McClain, R., 2000. Effect of fin spacing on convection in a plate fin and tube heat exchanger. Int. J. Heat Mass Transfer 43, 39–51.

Min, J.C., Webb, R.L., 2001. Numerical prediction of wavy fin coil performance. Enhanced Heat Transfer 8, 159–173.

Patanker, S.V., 1980. Numerical Heat Transfer and Fluid Flow. Hemisphere, Washington.

Tao, W.Q., 2001. Numerical Heat Transfer, second ed. Xi'an Jiaotong University Press, Xi'an.

Tao, W.Q., He, Y.L., 2002. Field synergy principle and its application in enhancing convective heat transfer and improving performance of pulse tube refrigerator, Part I. J. Xi'an Jiaotong Univ. 36, 1101–1105.

Tao, W.Q., Guo, Z.Y., Wang, B.X., 2002a. Field synergy principle for enhancing convective heat transfer—its extension and numerical verifications. Int. J. Heat Mass Transfer 45, 3849–3856.

Tao, W.Q., He, Y.L., Wang, Q.W., Qu, Z.G., Song, F.Q., 2002b. A unified analysis on enhancing single phase convective heat transfer with field synergy principle. Int. J. Heat Mass Transfer 45 (24), 4871–4879.

Tao, W.Q., Qu, Z.G., He, Y.L., 2004. A novel segregated algorithm for incompressible fluid flow and heat transfer problems—Clear (coupled and linked equations algorithm revised) part I: Mathematical formulation and solution procedure. Numer. Heat Transfer Part B 45, 1–17.

Tsai, S.F., Sheu Tony, W.H., 1998. Some physical insight into a two-row finned tube heat transfer. Comput. Fluids 27, 29–46.

Wang, S., Li, Z.X., Guo, Z.Y., 1998. Novel concept and device of heat transfer augmentation. In: Proceedings of the 11th International Conference of Heat Transfer. Taylor & Francis, Philadelphia, pp. 405–408.

Xi, G., Ebisu, T., Torikoshi, K., 1997. Differences in simulation with two- and three-dimensional models for finned tube heat exchangers. In: Transport Phenomena in Thermal Science and Process Engineering, Kyoto, Japan, 30 November–3 December 1997, pp. 755–760.

Xue, Wei, Min, Jingchun, 2004. Numerical predictions of fluid flow and heat transfer in corrugated channels. In: Proceedings of the 3rd International Symposium on Heat Transfer and Energy Conservation, Guangzhou, China, January 12–15, vol. 1, pp. 714–721.

Zeng, M., Tao, W.Q., 2004. Numerical verification of the field synergy principle for turbulent flow. J. Enhanced Heat Transfer 11, 411–416.